Rapid Communications

Microscopic model for magnetoelectric coupling through lattice distortions

D. C. Cabra,[1] A. O. Dobry,[2] C. J. Gazza,[2] and G. L. Rossini[3]

[1]*IFLySiB-CONICET and Departamento de Física, Universidad Nacional de la Plata, C.C. 67, (1900) La Plata, Argentina*

[2]*Facultad de Ciencias Exactas, Ingeniería y Agrimensura, Universidad Nacional de Rosario and Instituto de Física Rosario, Bv. 27 de Febrero 210 bis, 2000 Rosario, Argentina*

[3]*IFLP-CONICET and Departamento de Física, Universidad Nacional de la Plata, C.C. 67, (1900) La Plata, Argentina*

(Received 8 June 2019; published 28 October 2019)

We propose a microscopic magnetoelectric model in which the coupling between spins and electric dipoles is mediated by lattice distortions. The magnetic sector is described by a spin $S = 1/2$ Heisenberg model coupled directly to the lattice via a standard spin-Peierls term and indirectly to the electric dipole variables via the distortion of the surrounding electronic clouds. Electric dipoles are described by Ising variables for simplicity. We show that the effective magnetoelectric coupling which arises due to the interconnecting lattice deformations is quite efficient in one-dimensional arrays. More precisely, we show using bosonization and extensive density matrix renormalization group numerical simulations that increasing the magnetic field above the spin-Peierls gap, a massive polarization switch-off occurs due to the proliferation of soliton pairs. We also analyze the effect of an external electric field when the magnetic system is in a gapped (plateau) phase and show that the magnetization can be electrically switched between clearly distinct values. More general quasi-one-dimensional models and two-dimensional systems are also discussed.

DOI: 10.1103/PhysRevB.100.161111

Multiferroic materials exhibit a magnetoelectric (ME) coupling between their electrical and magnetic moments, a promising feature for device designs controlling magnetization with electric fields, or conversely electrical polarization with magnetic fields. They have been the subject of intense research in the last decade, a century later than the pioneering insight of Curie [1] and 50 years after the first theoretical prediction and experimental realization in Cr_2O_3 [2,3]. The current revival may be traced back to the simultaneous discovery of polarization and magnetization in bismuth ferrite $BiFeO_3$ [4] and gigantic magnetoelectric effects in rare-earth perovskite manganites $Tb(Dy)MnO_3$ [5]. Since then a series of exciting new materials and new microscopic descriptions have been developed (see the reviews [6–13], and references therein). Still, technologically useful multiferroic materials are very rare and constitute an active area of research.

Multiferroics are usually divided into two main groups, named type I and II, depending on whether ferroelectricity and magnetism have different or the same origin (see, e.g., [10,12], and references therein). Within the second group, in which ferroelectricity occurs in a magnetically ordered state, further distinction can be made if the magnetic order is collinear [10] or noncollinear [14,15].

Previous studies [16–23] have linked magnetostriction effects to magnetoelectricity, in particular for quasi-one-dimensional materials such as Ca_3CoMnO_6 [16], $R_2V_2O_7$ (R = Ni, Co) [17], double perovskites R_2CoMnO_6 (R = Er, Ho, Tm, Yb, Lu) [18], and also for more general cases such as magnetic E-type $HoMnO_3$ manganite [19,20], the nickelate family $RNiO_3$ (R = La, Pr, Nd, Sm, ..., Lu) (see, e.g., [21,22]), RMn_2O_5 manganites (R = Tb–Lu) [23], etc.

In the present Rapid Communication we focus on quasi-one-dimensional materials with collinear magnetic orders and propose an effective microscopic model in which the ME coupling is mediated by lattice distortions. Our main motivation arises from many different experiments where the coupling between magnetic moments, elastic distortions, and electric dipoles has been observed, in particular those in [24,25] where multiferroicity has been linked to magnetoelastic deformations in collinear spin models, which in turn produce a net electric polarization.

In this context we aim to provide a natural microscopic connection between the electroelastic and magnetoelastic effects and the resulting ME coupling. To this end we propose a model describing magnetic ions with spin $S = 1/2$, dipolar degrees of freedom, and deformations along a preferred axis, which allows for a description in terms of almost independent chains of octahedra, as is the case for [16,19,25], for example, or any other structural units. We find, among other effects, that this model allows for a switch-off of the electric polarization by applying a magnetic field, as well as for a magnetization jump induced by varying an electric field. These functionalities are key features that could lead to multiferroics-based technologies [26].

We then consider a chain of spin-1/2 magnetic ions [27] with the coupling to the lattice taken for simplicity as an adiabatic spin-Peierls term. We also assume that the ions whose motion produce the electric dipoles move in a deep enough double-well potential (the so-called order-disorder limit [28]) so that the orientation of electric dipoles is described by local Ising variables σ_i. Under longitudinal distortions δ_i we assume that dipoles remain located midway between magnetic ions. This granted, the coupling between elastic deformations and electric dipoles recognizes two contributions: one stems from the natural $1/r^3$ dependence of the dipole-dipole interaction and the other, central in our proposal, arises from a pantograph

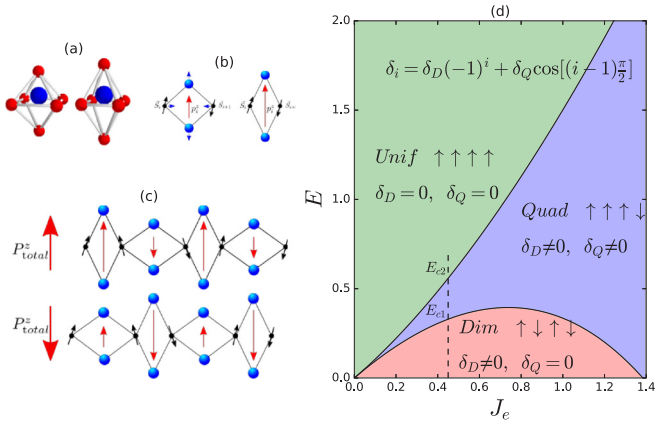

FIG. 1. Description of the pantograph mechanism and electroelastic phase diagram. (a) Typical distortion of basic structural units containing magnetic and electric variables. (b) Minimal model linking ion displacements (blue arrows) with spin and dipolar variables (black and red arrows), when a shear strain relates a distance reduction between magnetic ions with a dipolar strength enlargement. (c) The two possible dimerized chain configurations (related by one site translation, $\mathbb{Z}_2$), producing net polarizations in the presence of an antiferroelectric dipolar phase. (d) Dipolar phases and electroelastic distortions under an external electric field ($\alpha = 0$, $\beta = 0.2$). Following the dotted line at a given J_e one finds jumps in the polarization at E_{c1} and E_{c2}.

mechanism [29]. As changes in longitudinal bond lengths are related to the heights of the basic structural units, distortions change the width of the double-well potentials which in turn modify the dipolar strengths. A slight generalization could include the so-called bond-bending effects, where the magnetic superexchange is better described in terms of bond angles [19]; the conclusions of the present work would remain unchanged.

Assuming a preferred direction for the magnetoelastic distortions, a minimal geometry for the pantograph mechanism is depicted in Figs. 1(b) and 1(c), where for definiteness we set the dipoles to be perpendicular to the chain direction; octahedra in three-dimensional materials [Fig. 1(a)] undergo a similar process. In the following we analyze this simple geometry, considering the Hamiltonian

$$H_{ME} = H_{SP} + H_D, \tag{1}$$

where H_{SP} is the usual spin-Peierls Hamiltonian for $S = 1/2$ spins $\vec{S}_i$ and bond length distortions δ_i,

$$H_{SP} = \sum_i J_m(1 - \alpha\delta_i)\vec{S}_i \cdot \vec{S}_{i+1} + \frac{K}{2}\sum_i (\delta_i)^2 \tag{2}$$

with antiferromagnetic exchange J_m and elastic stiffness K, and H_D is the (long-range) electric dipolar energy. For transverse uniaxial dipoles H_D can be written as

$$H_D = \lambda_2 \sum_{i<j} \frac{1}{r_{ij}^3} p_i^z p_j^z, \tag{3}$$

where the distance $r_{ij} = r_{ij}(\{\delta_k\})$ between dipoles at links $j > i$ depends on distortions. The electric dipolar moments also depend on distortions by the pantograph mechanism, leading in a linear approximation to

$$p_i^z = p_0(1 - \beta\delta_i)\sigma_i. \tag{4}$$

External magnetic and electric fields along the z axis couple to the spins and dipoles, respectively, by

$$H_{\text{fields}} = -h\sum_i S_i^z - E\sum_i p_i^z. \tag{5}$$

In a general geometry, both α and β should be understood as phenomenological microscopic parameters, that could be fitted by experiments or by first-principles computations. The transversality condition on dipole orientations could be relaxed, either because of classical tilting or the inclusion of quantum fluctuations; in these cases our model requires further elaboration, to be reported in a forthcoming work.

In the case that screening makes negligible dipolar interactions beyond first neighbors, the Hamiltonian in Eq. (1) simplifies to

$$H_{ME} = J_m\sum_i (1 - \alpha\delta_i)\vec{S}_i \cdot \vec{S}_{i+1} + \frac{K}{2}\sum_i (\delta_i)^2 + J_e\sum_i \left[1 - \left(\beta + \frac{3}{2}\right)(\delta_i + \delta_{i+1})\right]\sigma_i\sigma_{i+1}, \tag{6}$$

where $J_e = \lambda_2(p^0)^2$ is the undistorted effective electric exchange coupling. Integrating out deformations would lead to a quartic expression coupling directly the magnetic and electric degrees of freedom, similar to that proposed in [27] to describe organic molecular solids. The microscopic derivation of this ME coupling will also be the subject of a forthcoming paper. We recall that the pantograph effect in Eq. (4) and the dependence of dipole-dipole electrostatic couplings on distance are at the root of the electroelastic coupling mechanism.

The electroelastic part of the Hamiltonian (setting $\alpha = 0$) is easily analyzed on classical grounds. Distinct dipolar configurations are favored according to the electric field and the different couplings considered, leading to a rich phase diagram. We show in Fig. 1(d) the electroelastic phases in the E-J_e plane for $\beta = 0.2$; K sets the energy scale. The lattice distortions can be analytically computed as a superposition of period two and/or period four harmonic distortions. The dimerized phase (*Dim*) has vanishing polarization at $E = 0$, slightly raising until a critical field E_{c1} where it jumps to nearly half of saturation in a quadrumerized phase [*Quad*; see Fig. 1(d)]. Distortions have contributions from both harmonics along this phase and the polarization also raises slightly, until a jump to saturation at a critical field E_{c2}.

On the other hand, the magnetoelastic part of the Hamiltonian (setting $J_e = 0$) is formally the same as the one used to describe the magnetoelastic effects in ferromagnetic materials [30]. In this work we focus on the extreme quantum case of spin $S = 1/2$ in one-dimensional chains and antiferromagnetic couplings, which has been widely studied mainly since the discovery of $CuGeO_3$ [31] and where the spin-Peierls effect is well established: the system is unstable towards a lattice deformation pattern commensurate with magnetic correlations. It then predicts a structural phase transition into a dimerized phase at zero magnetic field with the opening of a spin gap in the magnetic spectrum. This mechanism happens

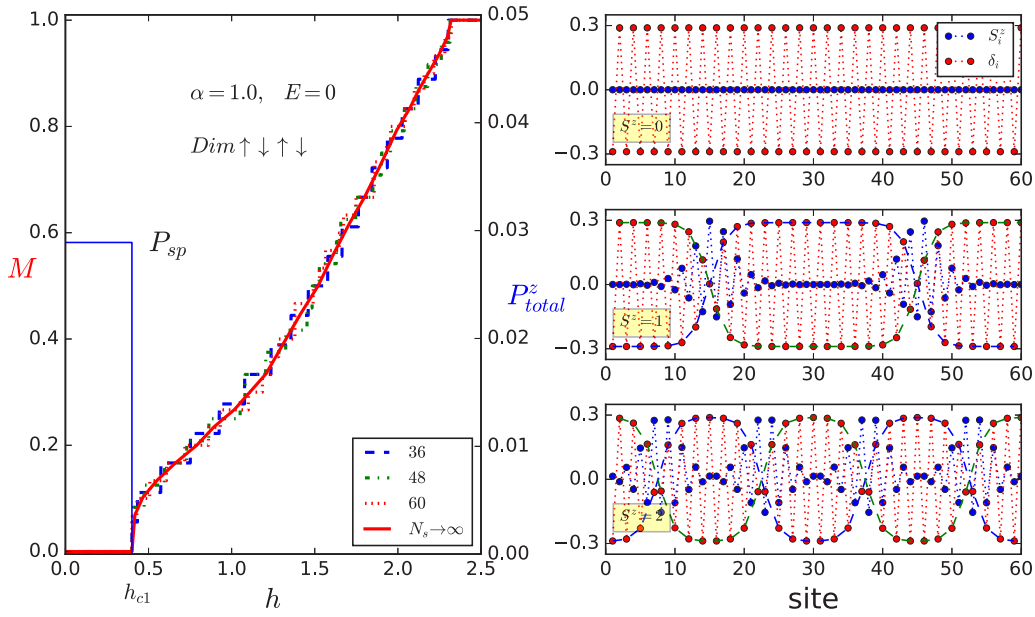

FIG. 2. Numerical results for $E = 0$ (setting $J_e = 0.5$, $\alpha = 1$, and $\beta = 0.2$). Left panel: Magnetization curve (infinite size extrapolation in solid red) and net polarization (in solid blue), both relative to saturation. A finite magnetic field is necessary to overpass the spin gap, dropping off the spontaneous polarization. Right panels: local magnetization and distortion profiles for $S^z = 0$ and the first two magnetized excitations $S^z = 1, 2$ indicating that equidistant soliton pairs (analytically fitted by dashed lines) proliferate as the magnetic field is increased.

to be effective also in frustrated chains, to give rise to spin gaps (magnetization plateaus) at nonzero magnetization M [32]. Magnetic excitations with $S^z = 1$ (magnons) on top of a given plateau split into a number of solitons which is fixed by the plateau magnetization ratio. These solitons repel each other and hence form a periodic array [33].

An efficient analysis can be made in the bosonization framework (see [32] for details). In this language the continuum expression for the spin energy density $\vec{S}_i \cdot \vec{S}_{i+1} \to \rho(x)$ reads [34]

$$\rho(x) = a\,\partial_x\phi + b : \cos(2k_F x + \sqrt{2\pi}\phi) : + \cdots , \qquad (7)$$

where ϕ is the bosonic field, $k_F = \frac{\pi}{2}(1 - M)$, M is the magnetization (relative to saturation), a and b are M-dependent nonuniversal constants, and the ellipses indicate higher harmonics. The magnetoelastic coupling will then be effective when distortion modulations are commensurate with spin energy density oscillations.

Our approach to the full Hamiltonian in Eqs. (5) and (6) is based on a self-consistent adiabatic procedure to minimize the energy for a given (classical) dipolar and (quantum) spin configuration, setting distortions as

$$\delta_i = \frac{1}{K}[J_e(\beta + 3/2)\langle\sigma_i\sigma_{i+1} + \sigma_{i-1}\sigma_i\rangle + J_m\alpha\langle\vec{S}_i\vec{S}_{i+1}\rangle - p_0 E\beta\langle\sigma_i\rangle] \qquad (8)$$

(with a subtraction of their average in order to fulfill a fixed length constraint). In this way we neglect both quantum and thermal fluctuations in δ_i; this approximation is valid in the low-temperature regime, when the phonon frequency is lower than the spin-Peierls gap. We have performed an iterative numerical analysis based on the density matrix renormalization group (DMRG) to solve the magnetic and electric sectors in the adiabatic equations (8), along the lines stated in [35] and implemented in a similar context in [32]. We have used periodic boundary conditions, keeping $m = 300$ states during up to more than 100 sweeps in the worst cases, getting truncation errors lower than $O(10^{-12})$.

The present model is capable of displaying the ME interplay. In particular, when spin-Peierls dimerization occurs at zero magnetic field and the magnetic subsystem is in a gapped phase with $M = 0$, one has $2k_F = \pi$ and the more relevant modulation term which is commensurate with the spin energy density oscillations reads $\delta(x) = \delta_D \cos(\pi x + q\pi)$, $q = 0, 1$.

For $E = 0$ the electric subsystem is in the antiferroelectric Ising regime and exhibits a spontaneous polarization $P^z_{\rm total} \equiv \frac{1}{p^0}\sum_i p^z_i = \sum_i \sigma_i(1 - \beta\delta_i) = \pm P_{\rm sp}$ where $P_{\rm sp} = \beta\delta_D N$. Notice that the polarization is extensive and spontaneous, with $\delta_D \neq 0$ due to the spin-Peierls effect. Moreover, the polarization has two possible orientations depending on the breaking of the translational symmetry of the magnetoelastic chain into $\mathbb{Z}_2$ as indicated in Fig. 1(c). This in turn induces a spontaneous breaking of inversion symmetry along the z axis. By increasing the magnetic field above the spin gap ($h > h_{c1}$) there occurs an incommensurate transition with the excitation of localized singlets into triplets, which decay into pairs of solitons. The double degeneracy of dipolar antiferroelectric configurations has a dramatic effect in the polarization: as solitons, for $E = 0$, form a regular array [33] interpolating between $q = 0, 1$, $P^z_{\rm total}$ vanishes identically.

Thus the magnetic transition causes a complete switch-off of electrical polarization, $P^z_{\rm total}(h > h_{c1}) = 0$. This effect could be observed in inelastic neutron scattering experiments.

The numerical results shown in Fig. 2 illustrate the polarization switch-off mechanism: the left panel shows the

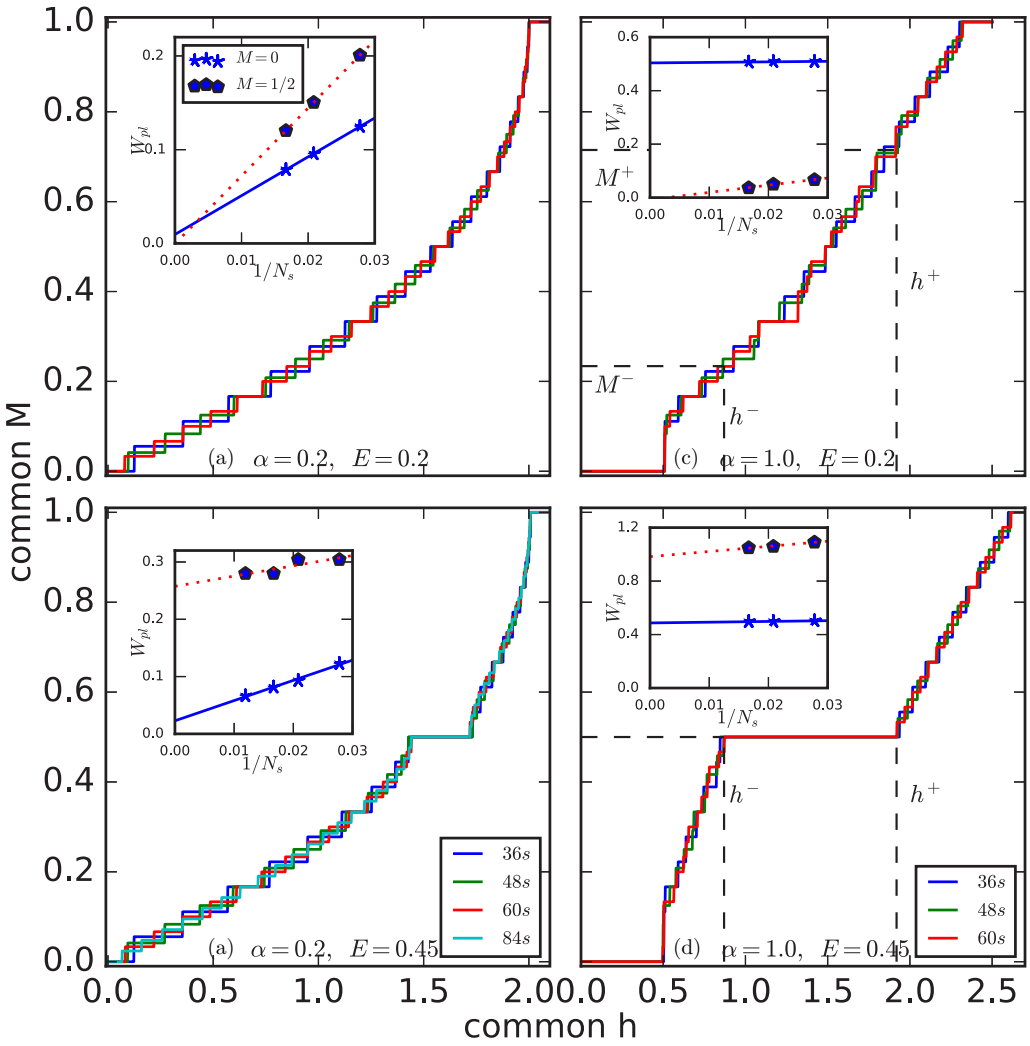

FIG. 3. Magnetization curves for $E \neq 0$ (setting $J_m = 1$, $J_e = 0.5$, and $\beta = 0.2$); the insets show the infinite length extrapolation of the main plateau widths, in order to assess their presence in the thermodynamic limit. A plateau at $M = 0$ is always present; when E drives the dipolar system into a quadrumerized phase a second plateau opens at $M = 1/2$. $h^{\pm}$, the lower and upper boundaries of the $M = 1/2$ plateau, are marked for later discussion (see Fig. 6).

presence of a magnetization plateau at $M = 0$ and a critical magnetic field h_{c1} to overcome it; the right panels show the spin and distortion configurations, as well as the dipolar background and the net polarization. For $M = 0$ the alternating distortions are in phase (say $q = 0$) along the chain, while for $S^z = 1, 2$ well-defined equidistant solitons produce regions with $q = 0, 1$ and a vanishing net polarization; the analytical expression for the first soliton pair, $\delta_i = \pm\delta_D \tanh(\frac{i-i_1}{\xi}) \tanh(\frac{i-i_1+N/2}{\xi})$, is indicated with dashed lines in the right middle panel.

The presence of a finite electric field $E < E_{c1}$ penalizes the region with dipoles and distortions having the same sign [see Eq. (5)], gluing the soliton-antisoliton pairs and producing a damping in the polarization switch-off effect (see Fig. 4, upper right panel).

Higher electric fields $E_{c1} < E < E_{c2}$ induce dipole flips, driving the electric subsystem to a $\uparrow\uparrow\uparrow\downarrow$ configuration. Being the distortions a superposition of period two and four harmonics, the presence of magnetization plateaus at $M = 0$ and $M = 1/2$ is anticipated. We have checked numerically that this picture remains qualitatively the same when the dipolar subsystem is coupled with magnetism ($\alpha \neq 0$), with a smooth renormalization of the phase boundaries in Fig. 1(d). Representative magnetization curves exhibiting plateaus, computed numerically from DMRG, are shown in Fig. 3, for values of $E = 0.2, 0.45$ and $\alpha = 0.2, 1.0$. One observes that the plateau at $M = 0$ is always present, while a second plateau opens at $M = 1/2$ when E drives the dipolar system into the quadrumerized phase. The plateau widths are enhanced by higher magnetoelastic coupling α.

Details on the quantum states at the $M = 0$ plateau and their magnetic excitations are shown in Fig. 4. We show distortion and magnetization profiles for low electric fields, at $S^z = 0$ (a) and first magnetized excitation (b). In the latter the continuous lines indicate the soliton profiles for $E = 0$, to be compared with the finite field profiles (dashed lines) that show the gluing of solitons. This gluing effect is more pronounced for electric fields in the quadrumerized phase (c),

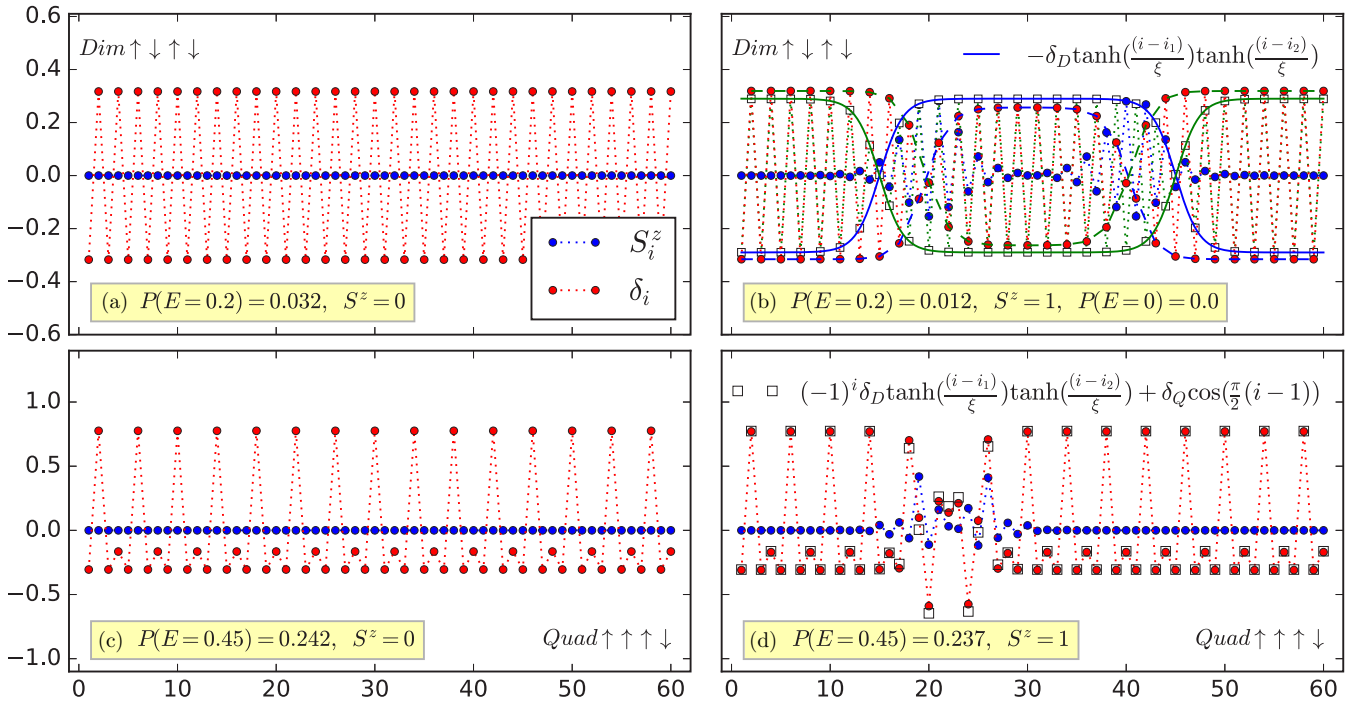

FIG. 4. Distortion and magnetization profiles at the $M=0$ plateau for $E\neq 0$ ($J_m=1$, $J_e=0.5$, $\alpha=1$, and $\beta=0.2$, in a $N=60$ sites chain with periodic boundary conditions). The differences in local dipolar profiles are clearly seen for E below or above E_{c1} [panels (a) and (c)]. The soliton-antisoliton pair for the first magnetic excitation is glued together by the electric field [panels (b) and (d)]; blue and green curves in panel (b) describe the repulsive soliton-antisoliton pair for $E=0$, added for comparison.

as seen in panel (d) where distortions are fitted with $\delta_i = (-1)^i\delta_D\tanh(\frac{i-i_1}{\xi})\tanh(\frac{i-i_2}{\xi})+\delta_Q\cos[\frac{\pi}{2}(i-1)]$, with $i_{1,2}$ indicating the soliton positions.

The plateau at $M=1/2$ has particular features not present in the spin-Peierls one at $M=0$. On the one hand, the magnetic wave function is compatible with an ordered direct product of singlets and spin-up sites, as depicted in Fig. 5. Magnetic excitations are simply given by magnons, that is, singlet-triplet transitions that do not decay into solitons (see Fig. 5, right panels). On the other hand, the quantum state is topologically nontrivial, as signaled by the even degeneracy of the entanglement spectrum [36]. This is an indication that within this $M=1/2$ plateau, the system belongs to a Haldane phase, topologically equivalent to the spin-1 Heisenberg model. This is different than the situation in the $M=0$ plateau, which is not topologically protected. We will further explore these points in a forthcoming paper.

The present pantograph model also describes the effects of an electric field on the system magnetization. Let us analyze the scenario in which both dimerized and quadrumerized phases appear as a function of E, e.g., by choosing $J_e=0.5$, $\beta=0.2$ [see Fig. 1(d)]. For $E_{c1}<E<E_{c2}$ the dipolar sector is quadrumerized and so is the lattice, which forces the magnetic sector to open a plateau at $M=1/2$, as clearly seen from the numerical results in Fig. 3. Choosing a background magnetic field h^- at the lower boundary of this plateau, the magnetization will jump from some value $M^-<1/2$ to $M=1/2$ as the electric field crosses E_{c1} from below; conversely, choosing h^+ at the upper boundary the magnetization will jump from some value $M^+>1/2$ to $M=1/2$. This ME response is schematically depicted in Fig. 6. Such a control of magnetization by an electric field is one of the goals of multiferroic technology developments [26].

Several quasi-one-dimensional materials showing multiferroicity have been studied in past years [11,16,24,25]. In most of these systems, a similar mechanism to the one proposed here seems to be relevant to describe the origin of the magnetoelectricity; though the spin ordering in some of them is of the type ↑↑↓↓ at zero magnetic field, spins may have a strong Ising anisotropy or take alternating different values along the relevant chain directions, etc. In order to describe these observed phenomena, one needs to consider further neighbors couplings between the neighboring spins and allow for higher spin $SU(2)$ representations or even consider Ising spins.

In the cases in which the magnetic moments can be treated as Ising variables, such as Ca_3CoMnO_6, the ANNNI (axial or anisotropic next nearest neighbours Ising) model has been proposed to describe the physics [16]. Even in such cases, the description of the process of magnetic depolarization must include excitations and/or quantum fluctuations. In this respect, our model is expected to provide the correct description of the transition and could be tested against experiments.

The extended J_1-J_2 model studied in [37] shows a $M=1/2$ plateau with period four symmetry breaking and dissociation of solitons as one increases or decreases the magnetization out of the plateau. In experiments done in $R_2V_2O_7$ ($R=$ Ni, Co) a similar situation has been observed, together with a sharp change in P on both sides of the 1/2 plateau [17]. In spite of these differences, the behavior of the magnetization and electric polarization in a magnetic field for spin-gapped

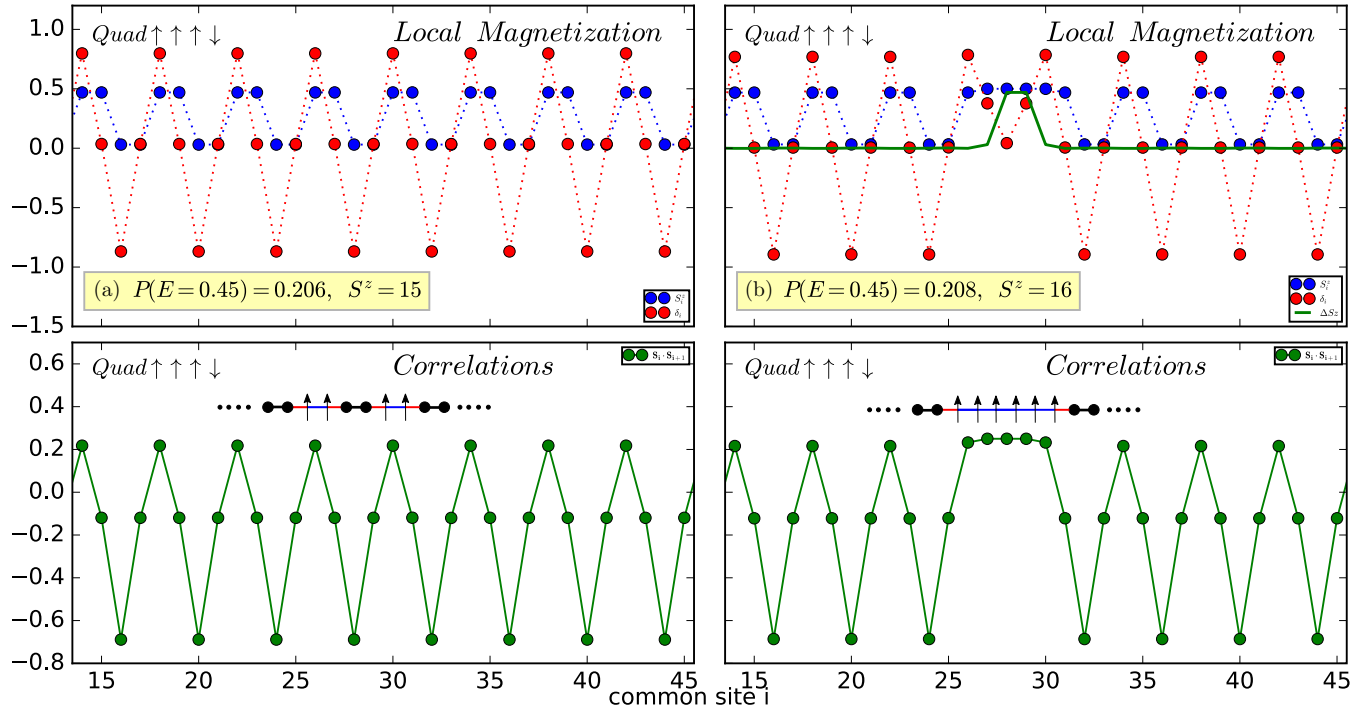

FIG. 5. Quantum state signatures of the $M = 1/2$ plateau (parameters as in Fig. 4, $E = 0.45$; we show again results for 60 sites, zoomed to visualize clearly the ordered direct product of singlets and spin-up sites). Local magnetization and nearest-neighbor correlations are compatible with a factorized quantum state of alternating up-up and singlet states. This is depicted graphically by black, red, and blue bonds indicating, respectively, singlet, weak antiferromagnetic, and ferromagnetic correlations. The lowest-energy spin excitation is a localized triplet; the green line in panel (b) indicates the local increase in S^z.

phases even at nonzero field (plateau phases) seems to be ubiquitous in all of the materials listed above.

The present mechanism is readily generalized to higher dimensions by considering the relevant structural units such as octahedra in perovskites, double tetrahedra in hexagonal manganites, etc. These units containing the magnetic atoms are arranged, say, in the corners of a square/cubic lattice and a kind of spin-Peierls mechanism can occur. Linking again the deformation of the lattice along a given preferential direction with the height of the basic unit [see Fig. 1(a)], the magnetoelectric coupling arises in the same way. Even in the case in which tunneling between double-well potential minima were not negligible, and electric dipoles were better described by a transverse Ising model, we expect our main conclusions to remain valid. Also higher spin magnetic ions, either classical or quantum, could be considered.

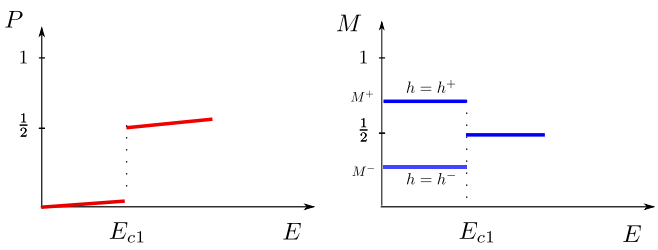

FIG. 6. Magnetoelectric response to the electric field in the quadrumerized scenario (schematic). Under appropriate applied magnetic fields $h^{\pm}$, as the electric field produces a polarization jump [see Fig. 1(d) at $J_e = 0.5$] the magnetization switches from $M^{\pm}$ to $M = 1/2$, the value at the plateau (see Fig. 3).

Recently in [38] multiferroic quantum criticality has been introduced phenomenologically via a Landau–Ginzburg-like effective action, with the suggestion that the quantum critical point could be tuned by varying external strain. It would be rather interesting to extend our present model to the higher dimensional quantum case to analyze their results microscopically, since strain plays a crucial role via the pantograph effect. As a test case, the one-dimensional full quantum version of the present model should be analyzed (work in progress).

Though the relation between striction and multiferroicity in quasi-one-dimensional systems has been discussed in several works [10,19,20], in most of the cases dipolar moments are not included as dynamical variables. In the present Rapid Communication we fill this gap by proposing a more general mechanism that includes electroelastic couplings via the distortion dependence of both local dipolar strengths and their interactions. The full Hamiltonian couples spins and electric moments via lattice deformations through the proposed pantographlike effect.

We hope that the present pantograph mechanism will shed light on the understanding of the microscopic origin of ME coupling in type-II multiferroics.

D.C.C. acknowledges useful discussions with M. Jaime, M. L. Medarde, M. Müller, and J. White. This work was partially supported by CONICET (Grants No. PIP 2015-813 and No. PIP 2015-364), Argentina.

[1] P. Curie, J. Phys. Theor. Appl. **3**, 393 (1894).
[2] I. E. Dzyaloshinskii, J. Exp. Theor. Phys. **10**, 628 (1960).
[3] D. N. Astrov, J. Exp. Theor. Phys. **11**, 708 (1960).
[4] J. Wang, J. B. Neaton, H. Zheng, V. Nagarajan, S. B. Ogale, B. Liu, D. Viehland, V. Vaithyanathan, D. G. Schlom, U. V. Waghmare, N. A. Spaldin, K. M. Rabe, M. Wuttig, and R. Ramesh, Science **299**, 1719 (2003).
[5] T. Kimura, T. Goto, H. Shintani, K. Ishizaka, T. Arima, and Y. Tokura, Nature (London) **426**, 55 (2003); T. Kimura, S. Ishihara, H. Shintani, T. Arima, K. T. Takahashi, K. Ishizaka, and Y. Tokura, Phys. Rev. B **68**, 060403(R) (2003).
[6] M. Fiebig, J. Phys. D: Appl. Phys. **38**, R123 (2005).
[7] S.-W. Cheong and M. Mostovoy, Nat. Mater. **6**, 13 (2007).
[8] R. Ramesh and N. A. Spaldin, Nat. Mater. **6**, 21 (2007).
[9] S. Dong, J.-M. Liu, S.-W. Cheong, and Z. Ren, Adv. Phys. **64**, 519 (2015).
[10] J. van den Brink and D. I. Khomskii, J. Phys.: Condens. Matter **20**, 434217 (2008).
[11] Multiferroic Materials: Properties, Techniques, and Applications, edited by J. Wang (CRC Press, New York, 2017). See, in particular, D. I. Khomskii in Chapter 1.
[12] Y. Tokura, S. Seki, and N. Nagaosa, Rep. Prog. Phys. **77**, 076501 (2014).
[13] S. Dong, H. Xiang, and E. Dagotto, Natl. Sci. Rev. **6**, 629 (2019).
[14] H. Katsura, N. Nagaosa, and A. V. Balatsky, Phys. Rev. Lett. **95**, 057205 (2005).
[15] M. Mostovoy, Phys. Rev. Lett. **96**, 067601 (2006); I. A. Sergienko and E. Dagotto, Phys. Rev. B **73**, 094434 (2006); A. B. Harris, T. Yildirim, A. Aharony, and O. Entin-Wohlman, *ibid.* **73**, 184433 (2006); A. B. Harris, *ibid.* **76**, 054447 (2007).
[16] Y. J. Choi, H.-T. Yi, S. Lee, Q. Huang, V. Kiryukhin, and S.-W. Cheong, Phys. Rev. Lett. **100**, 047601 (2008); R. Flint, H.-T. Yi, P. Chandra, S.-W. Cheong, and V. Kiryukhin, Phys. Rev. B **81**, 092402 (2010); M. Nishida, F. Ishii, and M. Saito, J. Phys. Soc. Jpn. **83**, 124711 (2014); V. S. Zapf, B. G. Ueland, M. Laver, M. Lonsky, M. Pohlit, J. Müller, T. Lancaster, J. S. Möller, S. J. Blundell, J. Singleton, J. Mira, S. Yañez-Vilar, and M. A. Señarís-Rodríguez, arXiv:1409.5072.
[17] R. Chen, J. F. Wang, Z. W. Ouyang, Z. Z. He, S. M. Wang, L. Lin, J. M. Liu, C. L. Lu, Y. Liu, C. Dong, C. B. Liu, Z. C. Xia, A. Matsuo, Y. Kohama, and K. Kindo, Phys. Rev. B **98**, 184404 (2018).
[18] J. Blasco, J. L. García-Muñoz, J. García, G. Subías, J. Stankiewicz, J. A. Rodríguez-Velamazán, and C. Ritter, Phys. Rev. B **96**, 024409 (2017); M. K. Kim, J. Y. Moon, S. H. Oh, D. G. Oh, Y. J. Choi, and N. Lee, Sci. Rep. **9**, 5456 (2019).
[19] I. A. Sergienko, C. Şen, and E. Dagotto, Phys. Rev. Lett. **97**, 227204 (2006).
[20] S. Dong, R. Yu, S. Yunoki, J.-M. Liu, and E. Dagotto, Eur. Phys. J. B **71**, 339 (2009).
[21] M. L. Medarde, J. Phys.: Condens. Matter **9**, 1679 (1997).
[22] S. Catalano, M. Gibert, J. Fowlie, J. Íñiguez, J.-M. Triscone, and J. Kreisel, Rep. Prog. Phys. **81**, 046501 (2018).
[23] L. C. Chapon, P. G. Radaelli, G. R. Blake, S. Park, and S.-W. Cheong, Phys. Rev. Lett. **96**, 097601 (2006).
[24] G. Giovannetti, A. Stroppa, S. Picozzi, D. Baldomir, V. Pardo, S. Blanco-Canosa, F. Rivadulla, S. Jodlauk, D. Niermann, J. Rohrkamp, T. Lorenz, S. Streltsov, D. I. Khomskii, and J. Hemberger, Phys. Rev. B **83**, 060402(R) (2011).
[25] S. V. Streltsov, A. I. Poteryaev, and A. N. Rubtsov, J. Phys.: Condens. Matter **27**, 165601 (2015).
[26] N. A. Spaldin and R. Ramesh, Nat. Mater. **18**, 203 (2019).
[27] M. Naka and S. Ishihara, Sci. Rep. **6**, 20781 (2016).
[28] A. D. Bruce, Adv. Phys. **29**, 111 (1980).
[29] The pantograph image has been used in a related magnetoelastic context by G. Radtke, A. Saúl, H. A. Dabkowska, M. B. Salamon, and M. Jaime, Proc. Natl. Acad. Sci. USA **112**, 1971 (2015).
[30] P. Deymier and K. Runge, Sound Topology, Duality, Coherence and Wave Mixing, *Springer Series in Solid-State Sciences* (Springer, New York, 2017), p. 188.
[31] K. Uchinokura, J. Phys.: Condens. Matter **14**, R195 (2002).
[32] C. J. Gazza, A. O. Dobry, D. C. Cabra, and T. Vekua, Phys. Rev. B **75**, 165104 (2007).
[33] T. Lorenz, B. Büchner, P. H. M. van Loosdrecht, F. Schönfeld, G. Chouteau, A. Revcolevschi, and G. Dhalenne, Phys. Rev. Lett. **81**, 148 (1998).
[34] F. D. M. Haldane, Phys. Rev. Lett. **45**, 1358 (1980).
[35] A. E. Feiguin, J. A. Riera, A. Dobry, and H. A. Ceccatto, Phys. Rev. B **56**, 14607 (1997).
[36] F. Pollmann, A. M. Turner, E. Berg, and M. Oshikawa, Phys. Rev. B **81**, 064439 (2010).
[37] K. Totsuka, Phys. Rev. B **57**, 3454 (1998).
[38] A. Narayan, A. Cano, A. V. Balatsky, and N. A. Spaldin, Nat. Mater. **18**, 223 (2019).